

**SENSITIVITY OF DIFFUSIVE-CONVECTIVE TRANSITION TO THE INITIAL  
CONDITIONS IN A TRANSIENT BÉNARD-MARANGONI PROBLEM**

**Eric Chénier\***  
**Christophe Desceliers**  
Université Paris-Est  
MSME - UMR 8208 CNRS  
5 bd Descartes  
77454 Marne-la-Vallée France

**Claudine Delcarte**  
**Benoît Trouette**  
Université Paris-Sud  
LIMSI - UPR 3251 CNRS  
Bât. 508 - Campus Universitaire  
91405 Orsay Cedex France

**Frédéric Doumenc**  
**Béatrice Guerrier**  
Université Pierre et Marie Curie, CNRS  
FAST - UMR 7608  
Bât. 502 - Campus Universitaire  
91405 Orsay Cedex France

**ABSTRACT**

*Sensitivity of a transient Bénard-Marangoni problem is studied using stochastic models to simulate the uncertainties of thermal initial conditions. Using different assumptions, three probabilistic models are developed and compared. Statistics are performed on flow velocities and temperatures. Transitions are examined with respect to the stochastic models.*

**NOMENCLATURE**

Bi Biot number  
 $e$  Fluid layer thickness  
 $H_{th}$  Global heat transfer coefficient  
 $k$  Thermal conductivity  
 $L$  Length of the fluid layer  
 $L_{ev}$  Latent heat of vaporization  
Ma Marangoni number  
 $p$  Dimensionless pressure  
Pr Prandtl number  
Ra Rayleigh number  
 $T_0$  Ambient temperature  
 $\vec{v}$  Dimensionless velocity vector,  $= u\vec{e}_x + v\vec{e}_y$   
 $V_i$  The  $i^{th}$  value of the vignettes  
 $\vec{x}$  Dimensionless spatial coordinates,  $= x\vec{e}_x + y\vec{e}_y$   
Greek symbols  
 $\alpha$  Thermal diffusivity,

$\beta_T$  Thermal expansion coefficient  
 $\Delta T$  Temperature scale  
 $\gamma$  Surface tension  
 $\Phi_{ev}$  Evaporation flux  
 $\mu$  Dynamic viscosity  
 $\rho$  Density  
 $\sigma_{X_\xi}$  Standard deviation of the stochastic value  $X_\xi$   
 $t$  Dimensionless time  
 $\theta$  Dimensionless temperature  
 $\Theta_\xi(x)$  Probabilistic condition for the initial temperature field  
Other symbols  
 $\langle X_\xi \rangle$  Mean value of the stochastic quantity  $X_\xi$   
 $\bar{X}_\xi$  Spatial average of the stochastic quantity  $X_\xi$   
Subscripts  
 $\xi$  Probabilistic variable

**INTRODUCTION**

The drying of a solution involves mass, momentum and energy exchanges between the liquid film and the surrounding gas. Phase change of the volatile component modifies the thickness of the fluid layer, the different concentrations in the solution close to the free surface, and therefore the local physical properties of the fluid mixture, and also the temperature at the interface due to the vaporization latent heat. These mass and thermal imbalances are able to create convective motions driven by buoyancy and capillary forces. Numerous authors have studied buoyant and capillary flows for volatile or nonvolatile

\*Address all correspondence to this author. Email: eric.chenier@univ-paris-est.fr

fluids, using the linear stability approach or direct numerical simulations [1–3]. Thus, more or less complicated numerical models have been erected but usually with the idea that steady flows would develop or by expecting quasi-steady regimes.

The key point of the drying of a solution is that the flow is transient by nature. From the fluid at rest, a transient diffusive regime takes place. During the temporal evolution, the dimensionless parameters may exceed temporarily critical values and thus perturbations can linearly grow around a transient basic state on a time interval before they decrease and disappear for long times.

The notion of stability thus needs to be revisited. One way to do is to freeze successively in time the basic solution and then to compute the instantaneous growth rate of the dominant disturbance. The interpretation of frozen time results may however be problematic, specially when the growth rate of the linear perturbation is larger than the characteristic time of the basic flow. Other methods, like the non normal approach, takes into account the transient character of the problem explicitly [4]. In this last method, the idea is to seek the initial disturbance that provides the maximum amplification of the kinetic or/and thermal energy. The critical parameter is then defined when this amplification exceeds one and reaches an arbitrary chosen value.

For experimental works or direct numerical simulations, the appearance of instabilities during the drying is also linked to the magnitude of the disturbances. Whereas the absolute control of perturbations is illusive in experimental works, it can almost be reached in numerical approaches by using very precise numerical schemes. Because such a numerical solution is in disagreement with experimental results where convection is observed, perturbations must be explicitly added in the numerical simulations in order to simulate the physical disturbances. The main question is how to reproduce these disturbances numerically, while they are usually out of control of experimentalists.

The aim of this paper is to study the sensitivity of fluid flows and transitions between diffusive and convective states as a function of initial disturbances. The paper is divided as follows. The thermal model of the drying of a solution is first introduced, then three uncertainty models for the thermal initial condition are described. The next section is devoted to the presentation of results before a conclusive section.

## PHYSICAL AND NUMERICAL MODELS

### Thermal model of drying - Transient Bénard-Marangoni problem

The simulations presented in this paper are based on drying experiments of a Polyisobutylene (PIB)/Toluene mixture. The

polymer solution at the ambient temperature is poured in a dish located under an extractor hood [5]. The physical model under consideration corresponds to the beginning of the drying only, when the convective motions have been experimentally shown to be driven by thermal gradients [5]. Thus for the sake of simplicity, the polymer mass fraction is assumed frozen, equal to its initial value, and the interface velocity is neglected. The evaporation at the free surface is taken into account through a global heat transfer coefficient  $H_{th}$  between the ambient air and the fluid interface. More details upon assumptions can be found in [6]. In a first attempt and in order to reduce the computational cost, the numerical analysis is restricted to two-dimensional problems. The liquid film is located in a rectangular domain of length  $L$  and thickness  $e$ . No-slip conditions are imposed on the adiabatic lateral and bottom solid walls. The dimensionless velocity  $\vec{v}(\vec{x}, t) = u(\vec{x}, t)\vec{e}_x + v(\vec{x}, t)\vec{e}_y$  and temperature  $\theta(\vec{x}, t)$  fields are solutions of the Navier-Stokes and energy equations under the Boussinesq approximation:

$$\begin{aligned} \vec{\nabla} \cdot \vec{v} &= 0 \\ \frac{\partial}{\partial t} \vec{v} + \vec{\nabla} \cdot (\vec{v} \otimes \vec{v}) &= -\vec{\nabla} p + \text{Pr} \nabla^2 \vec{v} + \text{RaPr} \theta \vec{e}_y, \\ \frac{\partial}{\partial t} \theta + \vec{\nabla} \cdot (\theta \vec{v}) &= \nabla^2 \theta \end{aligned} \quad (1)$$

with  $\text{Pr} = \mu/(\rho\alpha)$  and  $\text{Ra} = \rho g \beta_T \Delta T e^3/(\mu\alpha)$  are the Prandtl and Rayleigh numbers. The lengths are scaled by the thickness  $e$ ,  $e^2/\alpha t$  is the time,  $\alpha/e \vec{v}(\vec{x}, t)$  the velocity,  $\rho(\alpha/e)^2 p(\vec{x}, t)$  the dynamical pressure and  $T_0 + \Delta T \theta(\vec{x}, t)$  the temperature. The temperature scale  $\Delta T = (L_{ev} \Phi_{ev}(T_0))/H_{th}$  measures the difference between the temperature at the final equilibrium (constant and uniform temperature) and the ambient temperature  $T_0$  which is also the mean initial temperature. The boundary conditions write:

$$\begin{aligned} x = 0, \quad \vec{v} &= \vec{0}, & \frac{\partial \theta}{\partial x} &= 0 \\ x = L/e, \quad \vec{v} &= \vec{0}, & \frac{\partial \theta}{\partial x} &= 0 \\ y = 0, \quad \vec{v} &= \vec{0}, & \frac{\partial \theta}{\partial y} &= 0 \\ y = 1, \quad \begin{cases} \frac{\partial u}{\partial y} = -\text{Ma} \frac{\partial \theta}{\partial x} \\ v = 0 \end{cases} & & \frac{\partial \theta}{\partial y} &= -\text{Bi}(\theta + 1) \end{aligned} \quad (2)$$

where  $\text{Ma} = -\frac{e\Delta T}{\mu\alpha} \left( \frac{\partial \gamma}{\partial T} \right)$  and  $\text{Bi} = \frac{H_{th}e}{k}$  stand for the Marangoni and Biot numbers.

Using the properties of the Polyisobutylene (PIB)/Toluene [5], we can express the dimensionless parameters as a function of two physical parameters only, that were the control parameters used in the experiments, namely the thickness of the liquid film,  $e$ , and the viscosity of the solution,  $\mu$ . Notice that the viscosity can be adjusted by modifying the initial mass fraction of

the polymer in the mixture. The Rayleigh, Prandtl, Marangoni and Biot numbers write respectively  $Ra = 451e^3/\mu$ ,  $Pr = 12\mu$ ,  $Ma = 5850e/\mu$  and  $Bi = 0.2e$  with  $[e] = mm$  and  $[\mu] = mPa \cdot s$ .

### Uncertainty model for the thermal initial condition

As presented in Introduction, it is crucial to introduce disturbances into the numerical model in order to recover the transition between the diffusive and convective states which has been observed in experiments. Because it is very difficult, if not illusive, to reproduce the experimental disturbances, the idea is rather to consider a family of perturbations by using a stochastic approach. In this study, perturbations are imposed on the initial temperature field in the following way. The fluid is initially at rest:

$$\vec{v}(\vec{x}, t = 0) = \vec{0} \quad (3)$$

with a dimensionless temperature defined by some small probabilistic fluctuations,  $\Theta_\xi(x)$ , around the dimensionless null ambient temperature:

$$\theta_\xi(\vec{x}, t = 0) = 0 + \Theta_\xi(x) \quad (4)$$

For the sake of simplicity, the probabilistic fluctuation  $\Theta_\xi(x)$  only depends on  $x$  and is invariant in the  $y$ -direction. The stochastic behavior of the output  $X$  is measured through the mean value  $\langle X_\xi \rangle$ , the standard deviation  $\sigma_{X_\xi}$ , and the confidence interval 90% which is defined by the vigintiles (20-quantiles). We denote by  $V_1$  and  $V_{20}$  the first and last of the vigintiles. Statistical quantities are approximated by the Monte Carlo method which consists in performing many deterministic simulations,  $n$  for instance, with different random initial conditions  $\Theta_\xi^{(k)}(x)$ ,  $k = 1, \dots, n$ . The specific way to construct the initial conditions is described in the next subsections and the influence of stochastic models on temperature and flow field evolutions will be studied in the result section.

**Elementary approach** The simplest idea is based on the spatial discretization of the thermal initial condition  $\Theta_\xi^{(k)}(x)$  in the following way. By using  $N + 1$  discrete  $x$ -coordinates  $x_i = L/e \times i/N$ ,  $i = 0, \dots, N$ ,  $\{\xi_i, i = 0, \dots, N\}$  a family of random variables defined by the uniform and centered probability law on  $[-\sqrt{3}; \sqrt{3}]$  then

$$\Theta_\xi^{(k)}(x) = \sum_{i=0}^{N-1} H(x - x_i)H(x_{i+1} - x)\xi_i \quad (5)$$

with  $H(x)$  the Heaviside function. This approach excites independently the neighboring discrete values of the temperature

along the  $x$ -direction. Thus if the mesh size goes to zero, the temperature gradient evaluated at  $x_i$  tends to infinity what may affect the global convergence of the numerical scheme. Furthermore, this specific choice for the initial condition does not fit with the thermal boundary conditions at  $x = 0$  and  $x = L/e$  where no heat flux is imposed. At last in physical problems, the disturbances are probably spatially correlated, what is not taken into account in this elementary approach.

**Autocorrelation functions** In this approach, we assume that the disturbances should satisfy a specific autocorrelation function which is chosen in order to perform analytical calculations. This autocorrelation function writes:

$$R_1(x, x') = R_0 \exp\left(\frac{-|x - x'|}{\lambda}\right) \quad (6)$$

where  $\lambda$  is the dimensionless correlation length and  $R_0$  is a strictly positive real value characterizing the magnitude of the autocorrelation function, and as a result, it also controls the mean initial thermal energy injected by the disturbances. The associated stochastic process is defined by the Karhunen-Loève decomposition [7]:

$$\Theta_\xi(x) = \sum_{m=0}^{\infty} \sqrt{\beta_m} \xi_m \phi_m(x) \quad (7)$$

where  $\{\phi_m(x)\}$  is a Hilbert base in  $L^2([0, L/e])$ ,  $\beta_m > 0$  such that  $\beta_{i+1} \leq \beta_i$  and  $\lim_{n \rightarrow \infty} \beta_n = 0$ , and  $\{\xi_m\}$  is a family of random values which are chosen as being engendered by the uniform and centered probability law on  $[-\sqrt{3}; \sqrt{3}]$ . The functions  $\phi_m(x)$  are solutions of a differential equation

$$\phi_m''(x) + \frac{2\lambda R_0 - \beta_m}{\lambda^2 \beta_m} \phi_m(x) = 0 \quad (8)$$

Two different options are available to solve Eqn. (8), depending on whether the perturbations must fulfill the thermal boundary conditions at  $x = 0$  and  $x = L/e$  or whether the stochastic process must exactly satisfy the autocorrelation function (6).

If the Karhunen-Loève expansion must be compatible with the thermal boundary conditions, then  $(d\phi_m(x))/(dx) = 0$  for  $x = 0$

and  $L/e$  and we obtain:

$$\begin{cases} \phi_n(x) = \sqrt{\frac{2}{L/e}} \cos\left(\frac{n\pi}{L/e}x\right), & n \in \mathbb{N}^* \\ \phi_0(x) = \sqrt{\frac{1}{L/e}} \\ \beta_n = \frac{2\lambda R_0}{1 + \lambda^2 \left(\frac{n\pi}{L/e}\right)^2} \end{cases} \quad (9)$$

In that case, the autocorrelation function (6) is altered. The new autocorrelation function associated to the stochastic process is noted  $R_2(x, x')$  and writes:

$$R_2(x, x') = \sum_{n=0}^{\infty} \beta_n \phi_n(x) \phi_n(x') \quad (10)$$

with  $\phi_n(x)$  defined by (9).

If the thermal boundary conditions are released, the solution writes:

$$\begin{cases} \phi_n(x) = A_n \cos(\omega_n x + \chi_n) \\ A_n = \sqrt{\frac{2\omega_n}{\omega_n L/e + \sin(\omega_n L/e) \cos(\omega_n L/e + 2\chi_n)}} \\ \beta_n = \frac{2\lambda R_0}{1 + \lambda^2 \omega_n^2} \\ \chi_n = -\frac{\omega_n L/e}{2} + \frac{n\pi}{2} \\ \tan\left(\frac{\omega_n L/e}{2} - \frac{n\pi}{2}\right) = \frac{1}{\omega_n \lambda} \end{cases} \quad (11)$$

Notice that the last relation of system (11) leads to a transcendental equation which must be solved numerically.

### Numerical scheme

Equation (1) with the boundary conditions (2) are discretized by the finite volume method on staggered grids. Spatial derivatives are second order accurate. An implicit second order Euler scheme is used for time advance and the non-linear terms are approximated with a Adams Bashforth scheme. The coupling between the velocity and the pressure is achieved with a projection algorithm. Linear systems are solved with a Crout method using the red-black reordering technique. The random values used to construct the stochastic initial conditions are produced by the Mersenne Twister algorithm.

### RESULTS

Simulations are based on Polyisobutylene (PIB)/Toluene experiments [5]. The thickness of the fluid layer is fixed to

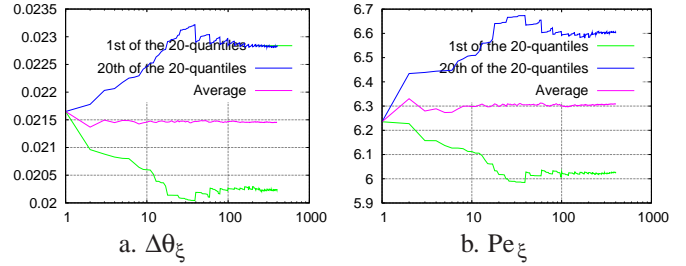


Figure 1. CONVERGENCE FOR THE ELEMENTARY APPROACH OF  $\langle \widehat{X}_\xi \rangle^{[i]}$ ,  $\widehat{V}_1^{[i]}$ , AND  $\widehat{V}_{20}^{[i]}$  AS A FUNCTION OF THE NUMBER OF MONTE CARLO RUNS ( $i$ ) FOR a.  $\Delta\theta_\xi$  AND b.  $Pe_\xi$ .

1 mm ( $Pr = 12$  and  $Bi = 0.2$ ) and the aspect ratio of the liquid film is equal to  $L/e = 20$ . Unless otherwise specified, results are presented using mean values associated with error bars corresponding to the confidence interval equal to 90%.

The mesh is regular and consists of  $800 \times 40$  control volumes. The time step is initialized equal to  $10^{-4}$  and increased by 1% at each iteration until it reaches  $10^{-3}$ .

For computations, the series defined by (7) are split to the 200<sup>th</sup> term and denoted by  $\Theta_\xi^{\{200\}}(x)$ ; the associated autocorrelation function is noted  $R^{\{200\}}(x, x')$ . In that case, the lowest dimensionless wave number of the probabilistic function  $\Theta_\xi^{\{200\}}(x)$  is equal to 0.20 and it is discretized on 8 control volumes of the mesh. Notice that the approximation errors  $\left| \frac{|R^{\{200\}}(x, x')|_{L^2([0;L/e]^2)}}{|R(x, x')|_{L^2([0;L/e]^2)}} - 1 \right|$  and  $\left| \frac{\langle \Theta_\xi^{\{200\}}(x) \rangle_{L^2([0;L/e])}}{\langle \Theta_\xi(x) \rangle_{L^2([0;L/e])}} - 1 \right|$  are respectively less than  $5 \cdot 10^{-3}\%$  and 0.5% for both models (9) and (11).

The convergence of the statistical quantity  $\chi^i(\vec{x}, t)$ , using  $i$  runs of the Monte Carlo method, is measured by the  $L^2([0;L/e] \times [0; 1]; [0; T])$ -norm:

$$\widehat{\chi}^{[i]} = \sqrt{\frac{1}{T} \int_0^T \frac{1}{L/e} \int_0^1 \int_0^{L/e} \chi^i(\vec{x}, t)^2 d\vec{x} dt} \quad (12)$$

where  $\chi^i(\vec{x}, t)$  could be either  $\langle X_\xi \rangle^i(\vec{x}, t)$ ,  $\sigma_{X_\xi}^i(\vec{x}, t)$ ,  $V_1^i(\vec{x}, t)$  or  $V_{20}^i(\vec{x}, t)$ . Figure 1 presents the convergence of both the mean value and the vigintiles for the Péclet number  $Pe_\xi(t) = \sqrt{|\overline{u_\xi^2}(\vec{x}, t)|_{L^2([0;L/e] \times [0;1])}}$  and the difference between the average temperatures at the bottom and at the interface  $\Delta\theta_\xi(t) = |\overline{\theta}_\xi(x, y = 0, t) - \overline{\theta}_\xi(x, y = 1, t)|$ , for  $\mu = 1 \text{ mPa} \cdot \text{s}$  ( $Ra = 451$  and  $Ma = 5850$ ).

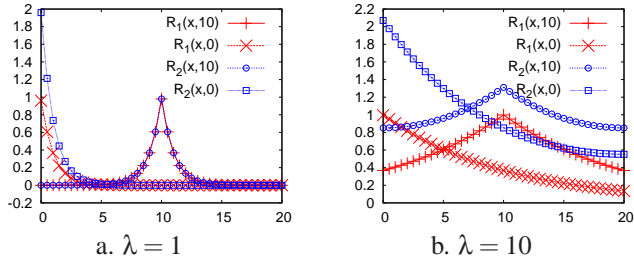


Figure 2. AUTOCORRELATION FUNCTIONS  $R_1(x, x_1)$  AND  $R_2(x, x_1)$  WITH  $x_1 = 0$  AND  $10$  AS A FUNCTION OF  $x$  FOR a.  $\lambda = 1$  AND b.  $\lambda = 10$ .

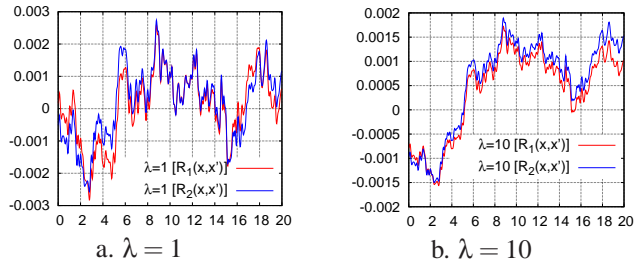


Figure 3. INITIAL THERMAL DISTURBANCES BASED ON  $R_1(x, x')$  AND  $R_2(x, x')$  AS A FUNCTION OF  $x$  FOR a.  $\lambda = 1$  AND b.  $\lambda = 10$ .

We consider that a good approximation of the statistical quantities are achieved with 200 runs of the stochastic thermal fields.

### The Karhunen-Loève model

Figure 2 shows the difference between the autocorrelation functions  $R_1(x, x')$  (Eqn. (11)) and  $R_2(x, x')$  (Eqn. (9)) for two  $x'$  values and two dimensionless correlation lengths  $\lambda$ . The two autocorrelation functions are all the more close than the correlation points are far from the boundaries and  $\lambda$  is small. The measure of the  $L^2$ -norm of  $R_1(x, x')$  and  $R_2(x, x')$  clearly illustrates this sensitivity: for  $\lambda = 1$ ,  $|R_1(x, x')/R_0|_{L^2([0;L/e]^2)} = 19.5$  and  $|R_2(x, x')/R_0|_{L^2([0;L/e]^2)} = 22$  whereas  $|R_1(x, x')/R_0|_{L^2([0;L/e]^2)} = 150$  and  $|R_2(x, x')/R_0|_{L^2([0;L/e]^2)} = 437$  for  $\lambda = 10$ . The calculation of the mean thermal energy injected at the initial time,  $|\langle \Theta_\xi(x)/\sqrt{R_0} \rangle|_{L^2([0;L/e])}$ , is noteworthy as well. Using the elementary approach or the model (11), we find 20. On the other hand by using (9) we obtain 21 (close to 20) for  $\lambda = 1$  but 30 for  $\lambda = 10$ . Therefore with the model compatible with the thermal boundary conditions, the modification of the correlation length multiplies by 3/2 the mean injected energy. Initial thermal perturbations are drawn in Fig. 3 for the same set of 200 random numbers. The two curves are close and even superimposed in the middle region, for  $\lambda = 1$ . As a conclusion, statistical solutions provided by the two Monte Carlo methods (9) or (11) are really comparable for a given  $\lambda$ -value provided that  $R_0$  is adjusted to get the same mean thermal energy for the initial condition.

### Convective flows

The following simulations were performed for  $\mu = 1 \text{ mPa} \cdot \text{s}$  ( $\text{Ra} = 451$  and  $\text{Ma} = 5850$ ) and a mean injected thermal en-

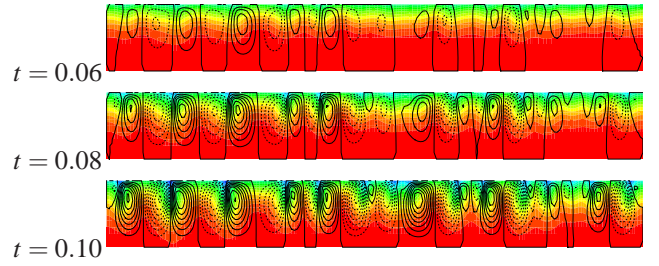


Figure 4. ISOTHERMS AND STREAMLINES AT 3 INSTANTS.

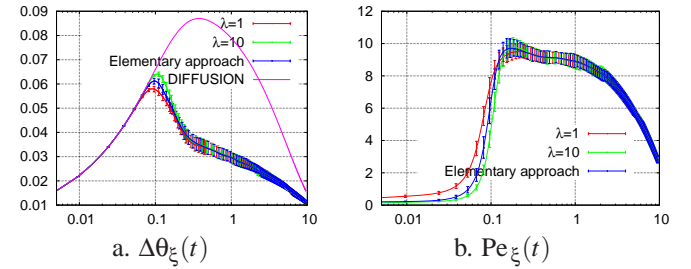


Figure 5. MEAN VALUES AND CONFIDENCE INTERVALS FOR a.  $\Delta\theta_\xi(t)$  AND b.  $\text{Pe}_\xi(t)$ .

ergy equals to  $2 \cdot 10^{-5}$ , namely a maximum intensity for the disturbance of order  $10^{-3}$  (see Fig. 3). For these Marangoni and Rayleigh numbers, the flow is driven by surface tension effects. A flow evolution is shown at three dimensionless times 0.06, 0.08 and 0.1 (0.6s, 0.8s and 1s) for model (9) and  $\lambda = 1$  (Fig. 4). We clearly distinguish the convection of the temperature field by the Marangoni cells and the evolution of the flow field.

Figure 5a illustrates the evolution of the mean values of the differences between the average temperatures at the bottom and at the free surface,  $\Delta\theta_\xi(t)$ , for the elementary approach, the Karhunen-Loève method (9) for  $\lambda = 1$  and  $\lambda = 10$ , and the purely diffusion problem ( $\text{Ma} = 0$  and  $\text{Ra} = 0$ ). As expected, the appearance of the convection reduces substantially the temperature gap between the top and bottom of the liquid layer because of the mixing. The departure from the diffusive solutions occurs between 0.07 and 0.09 (0.7s and 0.9s). From Fig. 5b, these times correspond to a Péclet number close to unit. We also note that convection becomes visible earlier with smaller correlation lengths and that the elementary approach based on uncorrelated disturbances is less effective to engender convection than the correlated case with  $\lambda = 1$  because the departure from the diffusion curve occurs later (Fig. 5a).

The local velocities at the free surface for three locations,  $x = L/(2e)$ ,  $x = L/(4e)$  and  $x = 3L/(4e)$  are drawn on Figs. 6a-6c. The mean values are small but confidence intervals are very large, what indicates an extreme sensitivity of the flow field with the initial conditions. Notice that the mean values and the medians (the 10<sup>th</sup> values of the vigintiles) are really close. However for  $t > 2$ , the mean flow seems to organize into more robust cells, anticlockwise for  $x = L/(4e)$  ( $\langle v_\xi \rangle(x = L/(4e), 1, t) < 0$ ) and

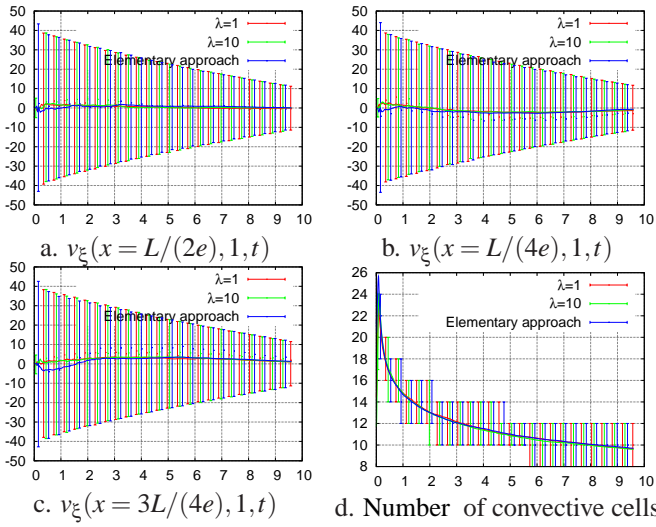


Figure 6. MEAN VALUES AND CONFIDENCE INTERVALS FOR THREE LOCAL VELOCITIES AND THE NUMBER OF CONVECTIVE CELLS.

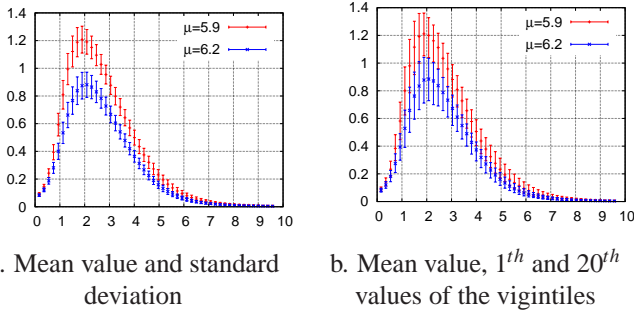


Figure 7.  $Pe_{\xi}(t)$  FOR  $\mu = 5.9 \text{ mPa} \cdot \text{s}$  AND  $\mu = 6.2 \text{ mPa} \cdot \text{s}$ .

clockwise for  $x = 3L/(4e)$  ( $\langle v_{\xi} \rangle(x = 3L/(4e), 1, t) > 0$ ). The center of the interface keeps a zero mean velocity. Except for very short times less than or of order 0.1, the different approaches give the same evolution for the number of cells at mid-thickness of the fluid layer (Fig. 6d). As expected, the number of cells decreases and should tend to zero when the solution converges to the final equilibrium state.

### Diffusive/Convective transition

The characterization of the flow is achieved by the Péclet number. If  $Pe_{\xi}(t) + \sigma_{Pe_{\xi}}(t) < 1$ , the solutions are considered purely diffusive. On the other hand, if  $Pe_{\xi}(t) - \sigma_{Pe_{\xi}}(t) > 1$ , the flow is said convective. The buffer zone between the diffusive and convective states defines the transition.

In the simulations presented here the layer thickness is fixed and the initial viscosity of the solution is variable. For a mean injected thermal energy equals to  $2 \cdot 10^{-5}$ ,  $\lambda = 1$  and model (11), the transition occurs for  $5.9 \text{ mPa} \cdot \text{s} < \mu < 6.2 \text{ mPa} \cdot \text{s}$  (Fig. 7a). Notice that the confidence intervals are almost similar to the standard deviations (Fig. 7b). The transition region does not

depend significantly on the model adopted and on the value of the correlation length  $\lambda$ . The most significant parameter is the value of the mean injected energy at the initial condition,  $\langle E_0 \rangle$ . For the model (11) and with  $\lambda = 1$ , the transition zone goes from  $5.9 \text{ mPa} \cdot \text{s} < \mu < 6.2 \text{ mPa} \cdot \text{s}$  for  $\langle E_0 \rangle = 2 \cdot 10^{-5}$  to  $4.4 \text{ mPa} \cdot \text{s} < \mu < 4.6 \text{ mPa} \cdot \text{s}$  for  $\langle E_0 \rangle = 2 \cdot 10^{-13}$ . By considering an average viscosity value of  $\mu = 5.3 \text{ mPa} \cdot \text{s}$ , the uncertainty is less than 20% whereas the energy injected was multiplied by  $10^8$  what corresponds to a factor 1000 between the highest and lowest magnitudes of the mean disturbances.

### CONCLUSIONS

We have studied, by means of three probabilistic approaches, the sensitivity of the thermal model in a drying process, to the uncertainties of the initial thermal conditions. No significant difference has really been observed on mean values, standard deviations or vigintiles for the evolution of the Péclet number, of some local velocities and of the average temperature variation between the top and bottom of the fluid layer. We have highlighted mixing effect of the fluid flow on the temperature field and that the convection occurs for a Péclet number value of unit order. We have also shown that the transition between the conductive and convective states was finally relatively few sensitive to the mean thermal energy injected at the initial condition.

### REFERENCES

- [1] Médale, M., and Cerisier, P., 2002. "Numerical simulation of Bénard-Marangoni convection in small aspect ratio container". *Numer. Heat Transfer A*, **42**, pp. 55–72.
- [2] Ozen, O., and Narayanan, R., 2004. "The physics of evaporative and convective instabilities in bilayer systems: linear theory". *Phys. Fluids*, **16**, pp. 4644–4652.
- [3] Moussy, C., Lebon, G., and Margerit., J., 2004. "Influence of evaporation on Bénard-Marangoni instability in a liquid-gas bilayer with a deformable interface". *Eur. Phys. J.*, **40**, pp. 327–335.
- [4] Doumenc, F., Boeck, T., Guerrier, B., and Rossi, M., In Press. "Rayleigh-Bénard-Marangoni convection due to evaporation: a linear non-normal stability analysis". *J. Fluid Mech.*
- [5] Toussaint, G., Bodiguel, H., Doumenc, F., Guerrier, B., and Allain, C., 2008. "Experimental characterization of buoyancy- and surface tension-driven convection during the drying of a polymer solution". *Int. J. Heat Mass Transfer*, **51**, pp. 4228–4237.
- [6] Touazi, O., Chénier, E., Doumenc, F., and Guerrier, B., 2010. "Simulation of transient Rayleigh-Bénard-Marangoni convection induced by evaporation". *Int. J. Heat Mass Transfer*, **53**, pp. 656–664.
- [7] Rozanov, Y., 1975. *Processus alatoires*. MIR, Moscou.